State Feedback Control for Adjusting the Dynamic Behavior of a Piezo-actuated Bimorph AFM Probe

by

Bilal Örün

A Thesis Submitted to the
Graduate School of Engineering
in Partial Fulfillment of the Requirements for
the Degree of

Master of Science
in
Mechanical Engineering

Koc University
January 2009

Koc University

Graduate School of Sciences and Engineering

This is to certify that I have examined this copy of a master's thesis by

Bilal Örün

and have found that it is complete and satisfactory in all respects,
and that any and all revisions required by the final
examining committee have been made.

Committee Members:

_____

Çağatay Başdoğan, Ph. D. (Advisor)

_____

Adem Levent Demirel, Ph. D.

_____

Levent Güvenç, Ph. D.

Date: _____

ABSTRACT

In this thesis, we adjust the transient dynamics of a piezo-actuated bimorph Atomic Force Microscopy (AFM) probe using a state feedback controller. This approach enables us to adjust the quality factor and/or the resonance frequency of the probe simultaneously. We first investigate the effect of feedback gains on the dynamic response of probe and then show that the time constant of the probe can be reduced by reducing its quality factor and/or increasing its resonance frequency to improve the scan error in tapping mode AFM.

ÖZET

Bu tezde, tam durum geri beslemeli kontrol yöntemiyle biri piezo olmak üzere iki katmanlı olan Atomik Kuvvet Mikroskobu (AKM) probunun geçiş dinamiği incelenmiş ve değiştirilmiştir. Bu yöntem sayesinde probun kalite faktörünü ve rezonans frekansını istediğimiz değerlere eşzamanlı olarak ayarlayabiliyoruz. Bunun için ilk olarak geri besleme kazançlarının probun dinamiğine olan etkisini inceledik ve sonra probun zaman sabitinin kalite faktörünü azaltarak ve/veya rezonans frekansını arttırarak düşürülebileceğini gösterdik. Zaman sabitinin düşürülmesi neticesinde AKM ile yapılan tarama sonuçlarında hatayı azalttık.

ACKNOWLEDGEMENTS

I would express my sincere gratitude to my thesis advisor Çağatay Başdoğan for his endless help and guidance during my study. His positive attitude and encouragement played a major role in my achievements and in the completion of this graduate study. I would also like to thank Prof. Adem Levent Demirel and Prof. Levent Güvenç for their participation in the thesis committee.

Great thanks to Çınar Ersanlı, Tolga Bayrak, İsmail Filiz and İlkin Kokal for being my home mates, social mates and buddies. I have great regard for Serkan Necipoğlu , Aydın Varol and Ilgar Veryeri, and I wish to extend my warmest thanks to them for their assistances and friendships both during and after lab hours. I gratefully thank to my friends Bekir Yenilmez, Gülşen Kamçı, Erdem Yüksel, Sina Öcal, and Umut Özcan for their helps and supports.

Finally, I would like to thank my father İsmail Örün, my brothers Metin Örün and İbrahim Örün for their beliefs and continuous supports on me.

Dedicated to my mother and sister.

TABLE OF CONTENTS

LIST OF TABLES

LIST OF FIGURES

Chapter 1

INTRODUCTION

The scan performance in a typical AFM system is related to the dynamical performance of the cantilever probe and the scanner. Given a piezo scanner with a high mechanical bandwidth and a robust controller that works with it, the scanning bandwidth and the image resolution obtained are mainly governed by the cantilever dynamics. Fantner et al. [1] emphasize that the maximum scan speed is determined by the spring constant, the effective mass of the cantilever, the damping of the cantilever in the surrounding medium, and the sample stiffness. Albrecht et al. [2] report that the response of a cantilever probe may be expressed in terms of a time constant $\tau = 2Q/\omega_n$, where Q is the quality factor and ω_n is the n^{th} resonance frequency of the probe. Hence, it is desirable to have low values of Q and high values of resonance frequency for faster response. Since the time constant of the probe is inversely proportional to its sensing bandwidth, increasing the Q factor of a cantilever probe limits its bandwidth. Albrecht et al. [2] show that for a cantilever probe in vacuum having high Q factor ($Q = 50000$) and a typical resonant frequency of 50kHz, its maximum available bandwidth is only 0.5Hz, which is not usable for most dynamic AFM applications. Mertz et al. [3] introduced a method that allows the active modification of the

cantilever's damping by the controlled increase or decrease of the apparent (effective) Q factor of the system, also known as the Q control today. In Q control, the positional movements of the probe are first measured using a sensor, then the signal is phase shifted in the time domain to obtain the corresponding velocity, finally the velocity signal is multiplied by a gain factor, G, and then added (subtracted) to (from) the actuation signal to change the effective damping (also the effective Q factor) of the cantilever probe. This can be achieved using an additional electronic circuit, including a phase shifter and a gain amplifier in the feedback loop. Sulchek et al. [4] showed that the sensing bandwidth of a scanning probe and its scan speed can be improved significantly by using a piezoelectric probe (instead of using a piezo-tube to actuate the probe in the Z-axis) and then by actively lowering the Q factor of the probe when scanning nano surfaces in air. Active damping allows the amplitude of the oscillating cantilever to respond to topography changes more quickly, but sacrifices the force sensitivity of the cantilever. Rodriguez and Garcia [5] develop an analytical model of a cantilever probe in the form of a mass spring damper system and investigate its dynamics under Q control in tapping mode. They emphasize the importance of the transients in the cantilever's response and show that the active response of a cantilever probe can be increased or decreased depending on the phase shift of the self-excitation. The optimum value of phase shift is at $\phi = \pm 90$ degrees (corresponds to pure velocity signal) because it does not modify the resonance frequency of the non-self-excited system, and at the same time it maximizes the Q factor. Moreover, they report that Q

enhancement reduces the maximum force exerted for the tip on the sample surface. Chen et al. [6] change the Q factor of a cantilever probe using Q control and show that increased effective Q promotes the attractive regime, improves imaging sensitivity, and results in less invasive imaging of soft biological samples. Numerical simulations performed by Kokavecz et al. [7] also support this argument. Ebeling et al. [8] compare imaging in liquid with and without the Q control and observe that heights measured with active Q control are reproducibly higher compared to the ones observed without Q enhancement. This effect is attributed to the reduction of tip-sample forces by Q control. In fact, Jaggi et al. [9] experimentally determined that the average tip-sample forces are reduced by Q enhancement. Despite these benefits, Q enhancement increases the transient time and adversely affects the scan speed. Holscher and Schwarz [10, 11] develop a mathematical model of a cantilever probe under Q control and determine the theoretical limits of the gain factor used for adjusting the effective Q factor of the probe in tapping mode AFM. They emphasize that adjusting the phase shift between the excitation and the cantilever oscillations to modify the Q factor of the probe could be problematic in real experiments and show that the gain factor is limited by $1/Q$ when the phase shift is ± 90 degrees and the effective Q factor of the probe becomes $Q_{eff} = 1/(1/Q \pm G)$, where G is the gain factor. When the same phase shift is increased to 0 or 180 degrees (corresponds to pure position signal), the native Q factor of the probe does not change but the resonance frequency is shifted by $0.5(f_n G)$, where $f_n = \omega_n / 2\pi$ is the resonance frequency of the probe.

Gunev et al. [12] suggested a new approach called adaptive Q control (AQC), in which the Q factor of a piezoelectric probe is adjusted on the fly during scanning. In standard Q control, achieving higher scan speeds with reduced tapping forces is not possible since the effective Q factor of the probe is set to a value that is lower or higher than its native one before scanning. In AQC, the controller modifies the Q factor of the probe on the fly to avoid the error saturation problem which typically occurs in scanning steep downward steps. The results of the experiments performed with an AFM setup show that the performance of AQC is superior to the standard Q control. Varol et al. [13] perform numerical simulations in SIMULINK to investigate nano scanning in tapping mode atomic force microscopy (AFM) under Q control. They focus on the simulation of the whole scan process rather than the simulation of cantilever dynamics and the force interactions between the probe tip and the surface alone, as in most of the earlier numerical studies. They discuss the tradeoff in setting Q factor of the probe in Q control, low values of Q cause an increase in tapping forces while higher ones limit the maximum achievable scan speed due to the slow response of the cantilever to the rapid changes in surface profile, and show the differences in scan performance at different settings using the iso-error curves obtained from the numerical simulations.

Most of the earlier studies on controlling the dynamical response of a cantilever probe have focused on adjusting its Q factor (i.e. damping). However, the stiffness and the mass of the

probe also play a crucial role in the response since they directly affect the resonance frequency ($\omega_n = \sqrt{k/m}$, where k and m are the effective stiffness and mass of the probe respectively). Viani et al. [14] show that the response time of a cantilever probe can be improved using smaller cantilevers. As a result, the mass of the cantilever is reduced, and the resonance frequency is increased, leading to a smaller time constant and faster response. However, using smaller cantilevers may cause difficulties while engaging sample surfaces and when scanning surfaces having large topographic variations. Varol et al. [13] show that scanning in an attractive regime using soft cantilevers with high effective Q factor results in a better image quality especially when scanning soft samples since the force sensitivity of the cantilever increases. Moreover, the risk of damaging biological samples is reduced. However, the response time of a soft cantilever with high Q factor is poor if the relation given by Albrecht et al. [2] for the time constant ($\tau = 2Q/\omega_n$) is considered.

Depending on the application, high or low values of Q factor and resonance frequency may be desirable. For example, if the purpose is to increase the scan speed in air, low Q and high ω_n is preferred. On the other hand, if a biological sample is to be scanned in liquid, Q factor must be enhanced for higher force sensitivity and the effective stiffness of the probe can be reduced to prevent damaging the sample. As obvious from the above discussion, adjusting the effective Q factor (by changing the damping) and the resonance frequency ω_n

(by changing the stiffness) of a cantilever probe is highly beneficial. In order to change the effective stiffness and damping of an AFM probe by altering the states of the probe simultaneously, state feedback control is necessary. The state space approach has been recently applied to modeling cantilever dynamics in AFM studies. Stark et al. [15] construct a state space model of a cantilever probe to investigate its dynamic response. They integrate the nonlinear forces between the tip and sample surface into the model as output feedback. This approach enables them to study the complex dynamics of different AFM modes through numerical simulations within one unified model. To capture the transient dynamics of a cantilever probe, Sebastian et al. [16] develop a state space model of the probe and then estimate the velocity of the probe using a "state observer". An observer is a computer implemented mathematical model that enables the estimation of a physical state that may not be measured directly. In typical AFM measurements, only the probe position is available and the velocity of the probe is not measured. Knowing the full state of the probe is helpful to better understand the tip-sample interactions and also opens the door for the implementation of new control strategies in dynamic AFM. In a later study, Sahoo et al. [17] show how the Q factor of the probe can be altered using a velocity observer. Authors emphasize the tradeoff between resolution and bandwidth in Q control and show that observer based Q control method provides greater flexibility in managing this tradeoff.

In this study, we present experimental methods for adjusting the effective Q factor and the resonance frequency of a cantilever probe through state feedback (Figure 1.1). To achieve this, we first measure the velocity of the oscillating probe using a Laser Doppler Vibrometer (LDV) and then obtain the position signal from the velocity signal via an analog integrator circuit. We finally, multiply the velocity signal with a gain G and the position signal with a gain H and then feed them back to the probe to change its effective damping and the stiffness, respectively. In order to make this change *simultaneously*, we utilize state feedback control. While changing the damping of the probe just affects its Q factor, changing the stiffness not only affects the resonance frequency but also the Q factor of the probe at the same time. Hence, state feedback approach is crucial for the calculation of the proper feedback gains. Using the calculated feedback gains, we perform scanning experiments to investigate the effect of state feedback on the image quality.

In addition to the scanning experiments, we further investigate the influence of state feedback on the dynamic response of the probe through numerical simulations performed in SIMULINK. For this purpose, we obtain a transfer function of the probe using the experimental data collected through frequency sweep. We then investigate the effect of feedback gains on the scan speed, the tapping forces, and image quality. We also show the tradeoff between the scan speed and the tapping forces under state feedback control, which

suggests that the feedback gains H and G must be selected carefully for optimum scan performance.

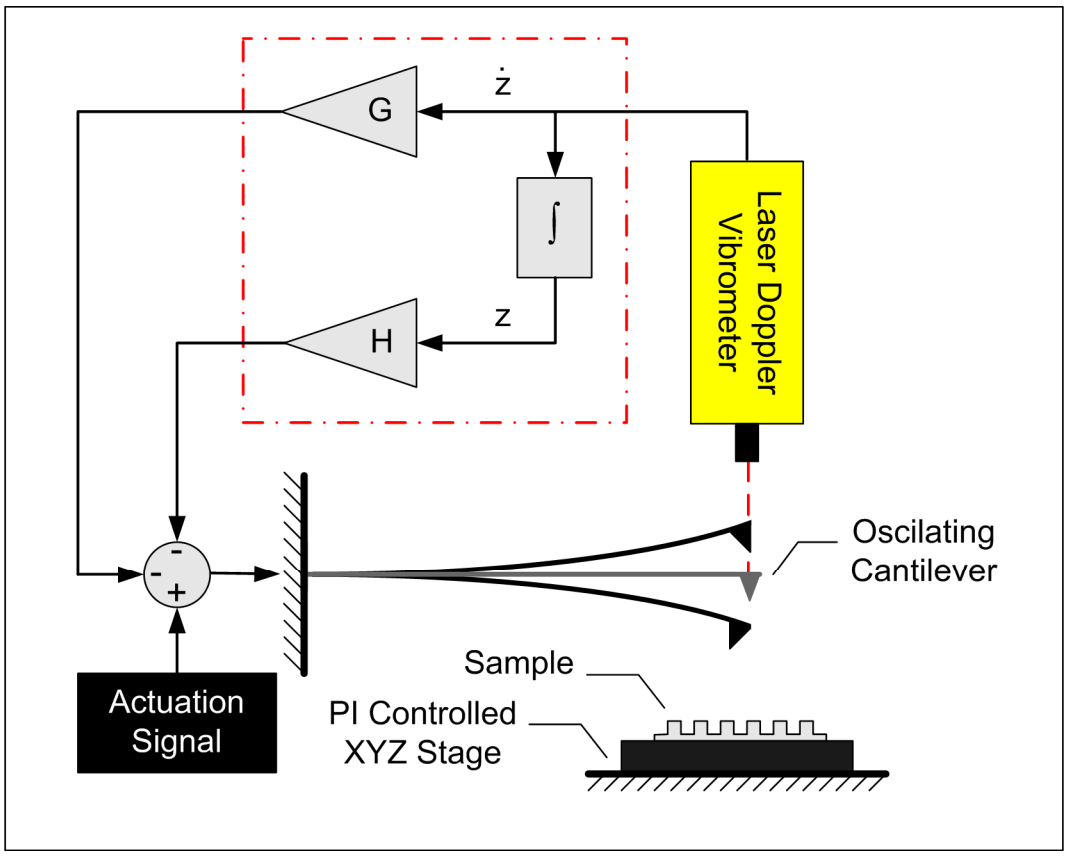

Figure 1.1: State feedback control of a piezo-actuated bimorph AFM probe. The feedback gains H and G enable us to operate the probe at a desired resonance frequency and Q factor. The area marked by the red dashed line is implemented as an analog circuit (see Figure 2.7).

Chapter 2

SETUP

The components of the setup for nano scanning are shown in a picture from the laboratory in figure 2.1. [18] A sample to be scanned is mounted on a XY raster scanning nano stage. The vibrations of the piezo-actuated bimorph probe, which is tapping on to the sample, is measured using a Laser Doppler Vibrometer (Polytec Inc., Germany) mounted on an optical video microscope system. A firewire camera (Point Grey Research Inc., Vancouver) and a light source are used for online visual imaging. The setup is capable of focusing the laser beam down to a spot size of ~2μm and positioning the spot on any point in the view area of the microscope using a 10X optical lens and the laser beam positioner (OFV-71). A signal conditioning circuit is employed to compute the root mean square (RMS) value of the vibrometer output signal. The circuit also enables the user to control the quality factor via velocity feedback and resonance frequency of the probe via position feedback. Using NI DAQ card the vibration amplitude of the bimorph probe is sampled into the computer in which the scan controller is running. Labview based scan control loop maintains constant vibration amplitude A_{set} by moving the nano stage in the Z-axis up and down during the

raster scanning of the sample. The negative image of the stage movements (Z-movements) equals the scanned topography.

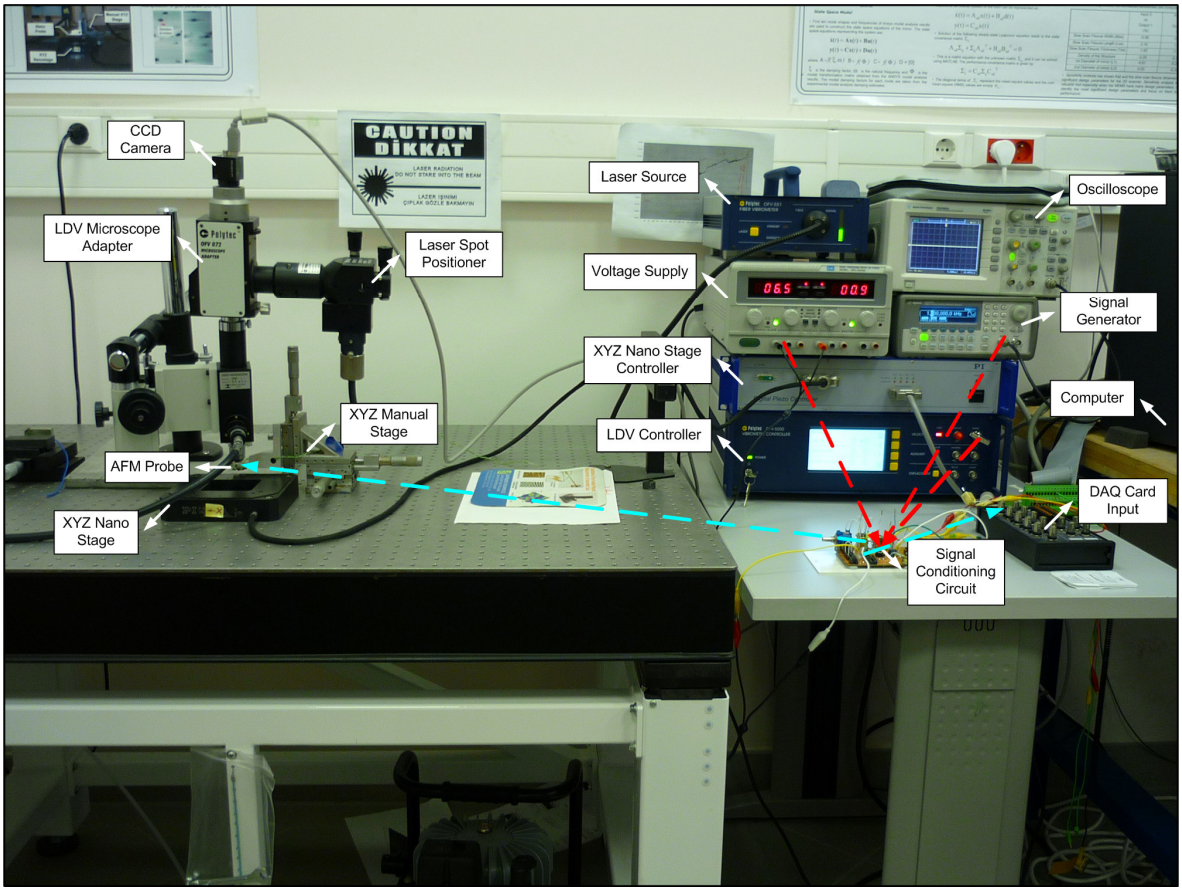

Figure 2.1: A photo of the nano scanning setup. Red dashed lines are the inputs (signal generator, LDV controller and voltage supply) of the signal conditioning circuit whereas the cyan dashed lines are the outputs (RMS value, and final actuation signal for the probe) of it.

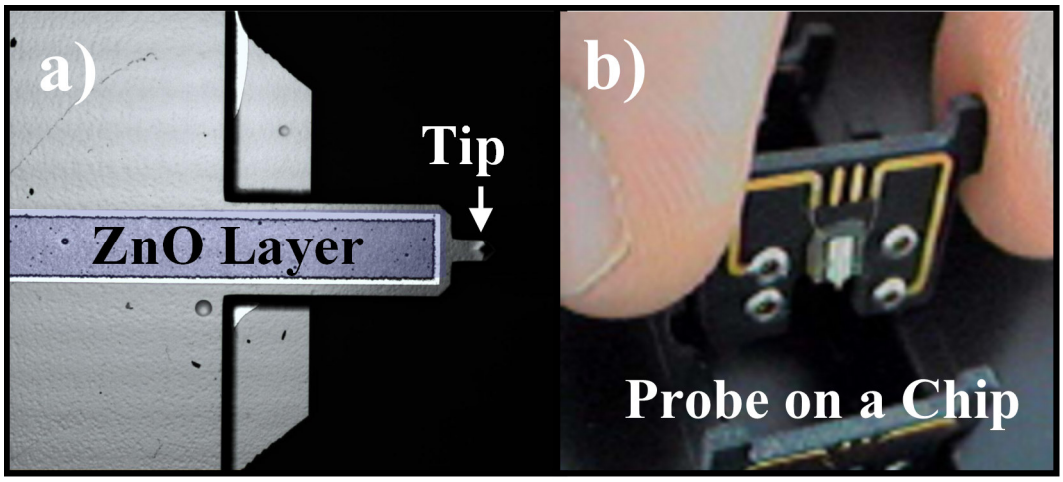

Figure 2.2: Picture of the AFM probe: a) Self actuated bimorph cantilever probe. b) Probe mounted on a chip.

2.1 Components of the Setup

2.1.1 AFM Probe

A commercially available self-actuated AFM probe (MPA-41100-10, Veeco Probes Inc., Santa Barbara, CA) is used for scanning the sample. The probe contains a ZnO stack (consisting of 0.25µm Ti/Au, 3.5µm ZnO, 0.25µm Ti/Au) at its base. This stack, along with the silicon cantilever, acts as a bimorph actuator for the vertical displacement of the probe tip (Figure 2.2.a). When voltage signals are applied to the pads at the fixed end of the cantilever, the ZnO layer bends up or down due to the piezoelectric phenomena. In this

way, the cantilever can be resonated by applying voltage signals at desired frequency. The probe which is already glued and on a chip (Figure 2.2.b) is mounted on a manual XYZ stage to bring it close to the sample surface.

2.1.2 Laser Doppler Vibrometer

A Laser Doppler Vibrometer, LDV, (Polytec GmbH, Germany.) is used for measuring the vibrations of the probe. The LDV having a bandwidth of 1.5GHz, measures the out of plane velocity of a point on the probe by collecting and processing the back scattered laser light. The fiber optic vibrometer is composed of the vibrometer controller (OFV-5000) and a fiber interferometer (OFV-551). The OFV-551 sensor head has a He-Ne red laser beam source (λ = 633 nm) utilized with a flexible fiber optic cable. The fiber optic cable delivers the laser light to the measurement point and collects the reflected light. Using a microscope system (VM-1V, Meiji Techno Co., Ltd, Japan) with 10X lens the laser beam is focused down to a spot size of ~2μm. The controller OFV-5000 processes the data collected from OFV-551 using a wide bandwidth velocity decoder (VD-02, which has four output scales (Table 2.1). The measurement data is acquired from the LDV controller (OFV-5000) in scaleable units of mm/s/V. Polytec OFV-71 and OFV-72 units are mounted between the microscope and the CCD camera (Flea, Point Grey Research Inc., Vancouver, Canada) to integrate the microscope system with the OFV-551 of the LDV. OFV-71 contains movable

mirrors to deflect the laser beam so that one can manually position the laser spot in the area of view of the microscope.

Measurement Scale LDV_{SCALE} (mm/s/V)	Resolution (μm/s)	Bandwidth (3dB value) (kHz)
5	0.8	250
25	2	1500
125	5	1500
1000	10	1500

Table 2.1: The dynamical characteristics of the vibrometer.

2.1.3 Optical Video Microscope

The optical microscope system consists of Meiji – 10X objective, VM-1V Video adaptable microscope unit with boom stand, a CCD camera and Meiji FL150 light source with halogen lamp. A field of view of 0.48mm X 0.36mm can be achieved with the VM-1V microscope using 1/3" CCD camera with 10X magnification objective. Meiji- S Plan M10X objective is an infinity corrected objective with 0.25 numerical apertures and a work distance of 9.4mm. The CCD camera is a Point Grey-FLEA CCD 1/3" IEEE-1394 camera

with 1024 X 768 resolutions (pixel size of 4.65μm X 4.65μm). Meiji FL-150 light source is a 150W halogen lamp used for inline illumination of the view area.

Polytec OFV-71 and OFV-72 units are mounted between the microscope and the CCD camera to integrate the microscope system with the OFV-551 of the LDV. OFV-71 contains movable mirrors to deflect the laser beam so that one can manually position the laser spot in the microscopes view area. An adjustable filter in OFV-72 reduces the intensity of the laser spot going to CCD cam which is very helpful when observing mirror like surfaces.

2.1.4 Signal Conditioning Circuit

The signal conditioning circuit consists of an RMS converter, a variable phase shifter, an integrator, two voltage multipliers for state feedback control, and two voltage dividers for adjusting feedback gains. (See figures 2.3, 2.4, 2.5, 2.6, and 2.7) The working principle of tapping mode scanning relies on the detection and control of the vibration amplitude of a scanning probe. The LDV is focused on the nano probe to measure its out of plane vibration velocity using Doppler phenomena. Due to the time spent during digital signal processing (DSP), there exists a constant time delay between the actual velocity and vibrometer output, which results in a phase shift between actual velocity and vibrometer

output. The delay circuit (variable phase shifter) in the system eliminates the time delay caused by the DSP of the LDV controller.

The LDV measures only vibration velocity V_{probe} of the nano probe in volts. Since the control loop requires exact vibration amplitude (A_p) of the probe, an analog RMS converter (AD536AJH) is used to make the conversion from V_{probe} to V_{rms}. The relation between V_{probe}, V_{rms} and A_p is given as:

$$V_{rms} = \frac{V_{probe}}{\sqrt{2}} \tag{2.1}$$

$$A_p = \frac{LDV_{scale} \cdot V_{rms} \cdot \sqrt{2}}{2\pi f} \tag{2.2}$$

RMS Converter: The RMS converter bases on an AD536AJH integrated circuit computes the true root mean square level of a complex ac (or ac plus dc) input signal and gives an equivalent dc output level. The true RMS value of a waveform is a more useful quantity than the average rectified value since it relates directly to the power of the signal. The RMS value of a statistical signal also relates to its standard deviation. Capacitor, C_{AV}, sets the averaging period. The value of this capacitor determines the low frequency ac accuracy, ripple level and settling time. If the input is a slowly varying dc signal, the output of the

circuit will track the input exactly. At higher frequencies, the average output of the RMS circuit will approach the RMS value of the input signal. The actual output of the circuit will differ from the ideal output by a dc (or average) error and some amount of ripple. The dc error is dependent on the input signal frequency and the value of C_{AV}. The ac component of the output signal is the ripple. By setting the value of the capacitor C_{AV} large we can reduce the ripple, since the ripple is inversely proportional to C_{AV}, a tenfold increase in this capacitance will affect a tenfold reduction in ripple. The primary disadvantage in using a large C_{AV} to remove ripple is that the settling time for a step change in input level is increased proportionately.

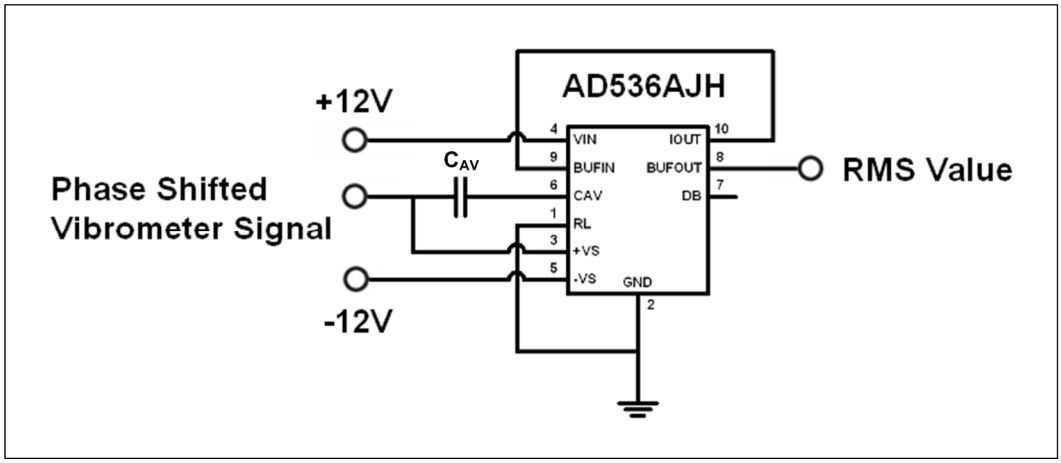

Figure 2.3: RMS to DC converter circuit.

Phase Shifter: In order to adjust the phase of the measurement signal a phase shifting circuit (delay circuit) is built. There are several ways to introduce an analog delay into a signal channel. In this work the delay was created using an active circuit (LF351 Opamp). In this approach a single resistor and capacitor controls the delay line. R in the circuit was set using a potentiometer R_{var}. This part enables the user to adjust the phase shift when needed.

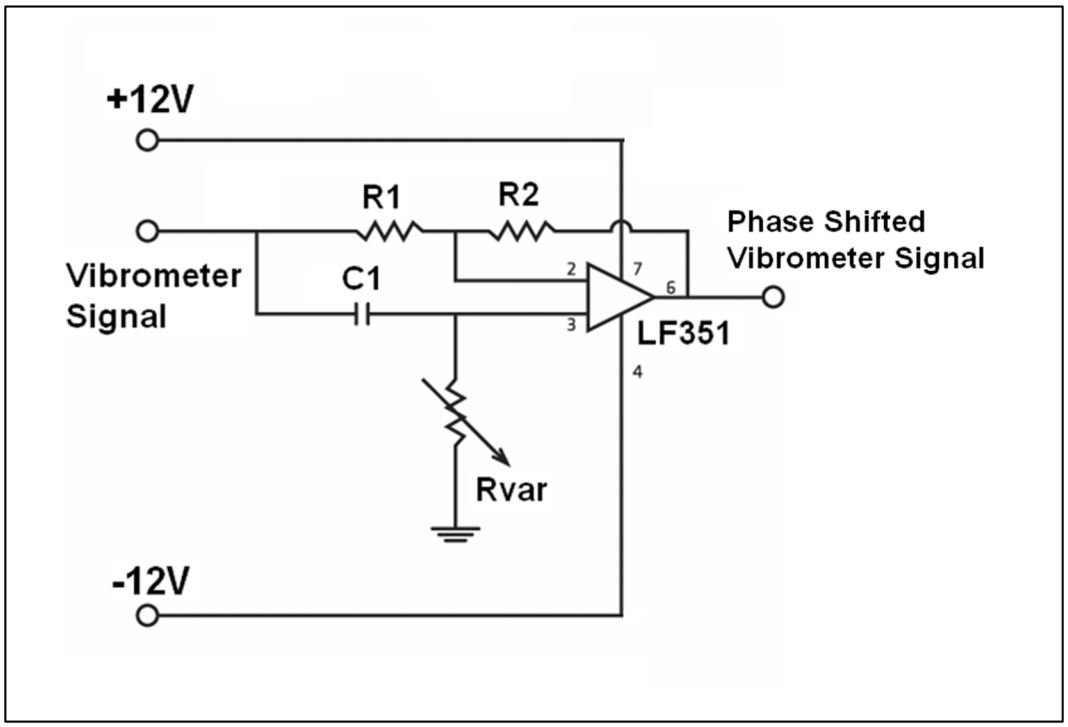

Figure 2.4: Phase shifter circuit.

Integrator: An inverter is basically a modified inverting amplifier circuit in which the output voltage waveform is the integral of the input voltage waveform. The relationship of current through (i_{C2}) and voltage across (v_{C2}) the capacitance *C2* is;

$$v_{C2}(t) = -\frac{1}{C2}\int i_{C2}(t).dt = -\frac{1}{R3C2}\int v_{C2}(t).dt \qquad (2.1)$$

Equation 2.1 indicates that the output voltage is scaled version of the integral of the input voltage. In other word, output voltage is directly proportional to negative integral of input voltage and inversely proportional with time constant *R3C2*. The factor $1/R3C2$ is known as integrator gain constant and has a dimension of frequency. In a practical integrator circuit, a large resistance *R4* in parallel with *C2* is connected in order to increase the stability. In fact the input signal will be integrated properly if the time period τ of the signal is larger than or equal to *R3C2*.

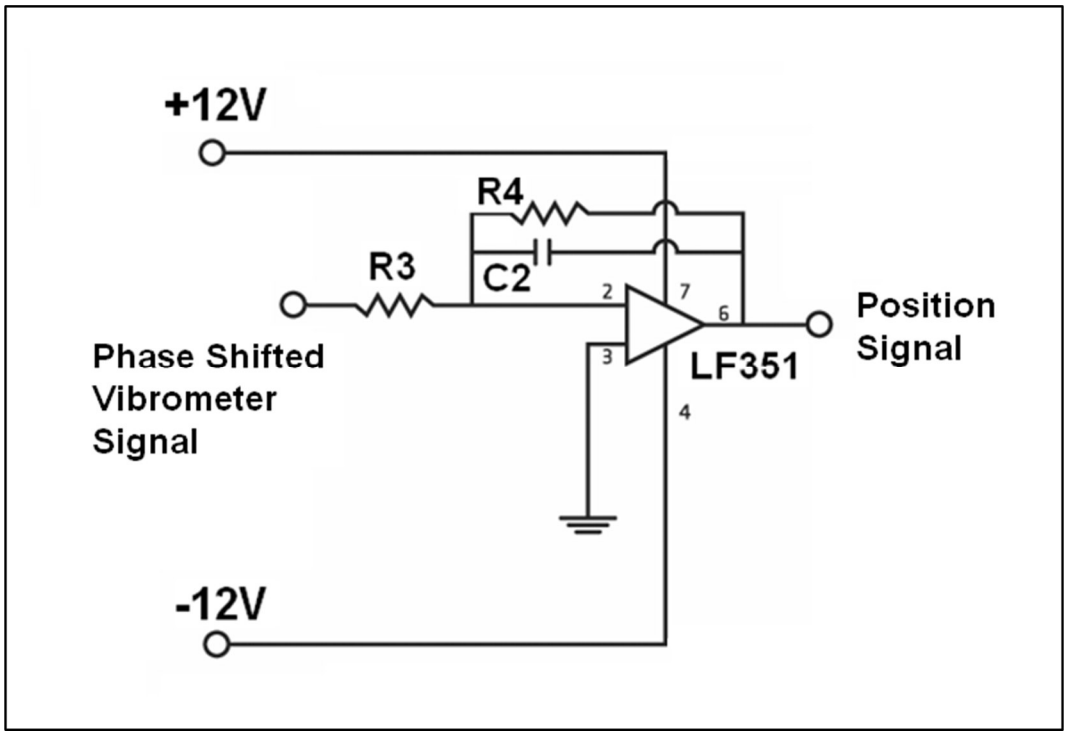

Figure 2.5: Analog integrator circuit.

Analog Voltage Multiplication: Analog voltage multiplication circuit enables the system to continuously scale vibrometer signal according to the each state feedback gain. In our work, analog voltage multiplication circuit is based on an AD633JN (Analog Devices) integrated circuit having the transfer function $W = [X * Y]/10 + Z$ (Figure 2.6). Where, Z is $Fsin(\omega t)$ actuation signal from the signal generator at or close to the resonant frequency of the probe, X is phase corrected velocity signal coming from LDV and phase shifter or position signal coming from the integrator, and Y is feedback velocity or position gain (G,

H) coming from voltage divider in the circuit shown in figure 2.7 for velocity feedback and *W* is the final actuation signal sent to the probe for operation under state feedback control.

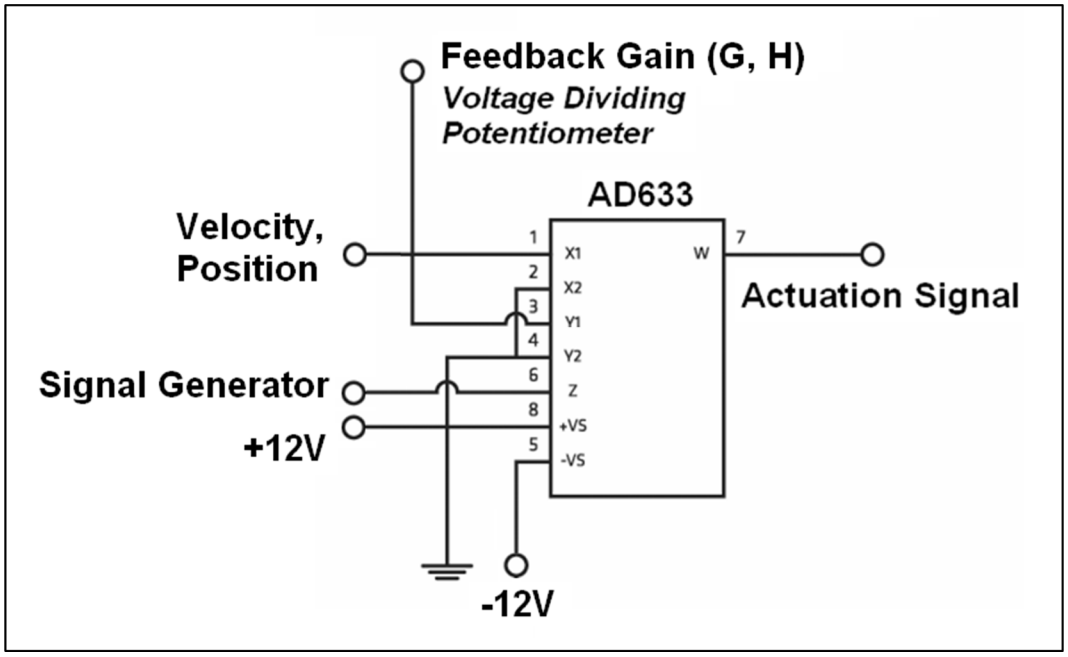

Figure 2.6: Voltage multiplication circuit.

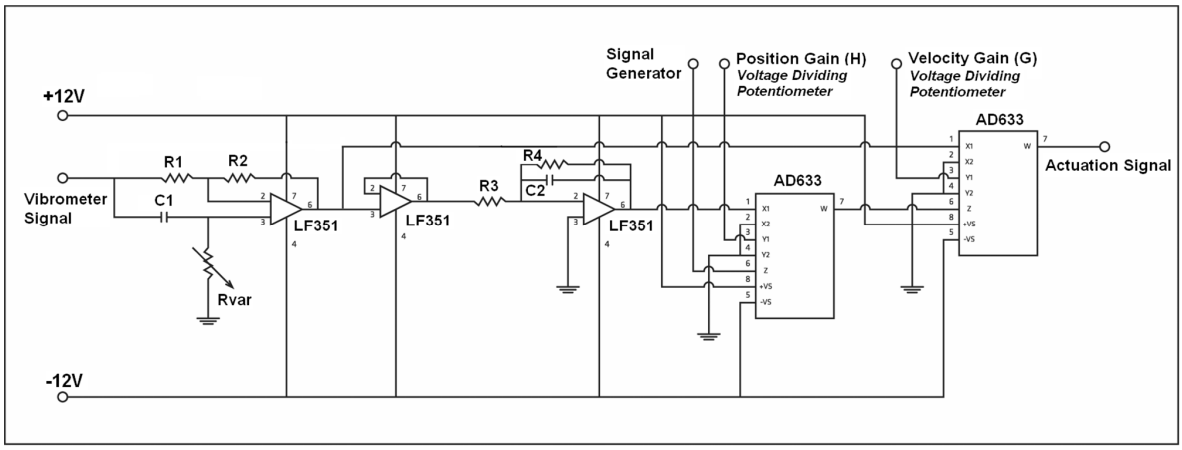

Figure 2.7: Final design of the signal conditioning circuit.

2.1.5 XYZ Scanning Nano Stage

All movements of the sample surface relative to the probe tip is controlled using a nano stage (PI Inc, Germany, Model No: P-517.3CD) with a digital controller unit (E-710.P3D). The nano stage has a travel range of 100nm X 100nm X 20nm (nominal resolution is 0.1nm) and an integrated capacitive sensor for precise positioning. The digital controller of the stage is connected to a digital data acquisition card (NI PCI-DIO-96) via parallel input output port running a high speed servo loop at 0.2ms/cycle. The usage of a digital nano stage brings high accuracy positioning with velocity controlled motion, noiseless operation, and high accuracy measurement of XYZ position. Moreover, it significantly reduces the

nonlinearity and creep seen in commercial atomic force microscopes during raster scan when a PZT tube is used as the positioning device.

2.1.6 Data Acquisition Hardware

Data acquisition cards are the most important hardware equipment in a computer controlled system since they are used in the control loops and information transfer. Two DAQ cards are used in the nano scanning setup. One 96 channel digital input-output card PCI-96 DIO (National Instruments Inc.) does the parallel communication with the nano stage. This card is installed into the computer which is running scan controller. Using this DAQ card, XY raster scanning and Z-controlled movement of the stage is achieved. Communication with the nano stage is done via Labview blocks and C/C++ libraries which are provided by the manufacturer of the stage. The second DAQ card PCI-6034E (National Instruments Inc.), which has Analog Input capability, is used to capture the RMS signal coming from the signal conditioning circuit. This card is installed into the computer running scan controller, too. 200kS/s sampling rate can be achieved using this DAQ card when using only one channel. In case of sampling with multiple channels, sampling rate is divided by the number of channels used for sampling. Sampling rate is the one of the factors limiting scan speed because the control loop cannot run faster than time between two samples.

2.1.7 Peripherals

In addition to the computer running the scan controller, one Agilent 33220A 20 MHZ function generator and Agilent DSO3062A oscilloscope is used to visualization and generation of signals. Both devices are connected to computer using 82357A USB/GPIB interface.

2.1.8 Software

The software used in this setup is a Labview based control loop which consists of a block diagram side and control panel side. Using this software, the user can easily set all of the parameters used in the tapping mode scanning, which are scan speed and scan line length in X and Y directions, A_{SET} is the desired tapping amplitude, PID control parameters and the name and location of the .txt file to record the data.

Chapter 3

CANTILEVER DYNAMICS

3.1 Cantilever Model

If we model the probe as a mass spring damper system vibrating under the influence of external forces, then its equation of motion can be written as:

$$m\ddot{z} + b\dot{z} + kz = F(t) \tag{3.1}$$

where, *m*, *b*, and *k* represent the effective mass, damping, and the stiffness of the probe respectively and *F(t)* represents the sinusoidal force applied to the probe tip for actuation. The transfer function between the force applied to the probe tip, *F(s)*, and the position of the probe tip, *z(s)*, can be written in Laplace domain as:

$$\frac{z(s)}{F(s)} = \frac{1/m}{s^2 + (b/m)s + (k/m)} \tag{3.2}$$

Now, if we consider a linear relation between the voltage applied to the piezo layer of the probe and the corresponding force generated at the probe tip, $F(s) = B_0 V(s)$, where B_0 is a constant, then the transfer function between the voltage applied to the piezo layer, $V(s)$, and the tip position, $z(s)$, can be written as:

$$\frac{z(s)}{V(s)} = \frac{B_1}{s^2 + A_1 s + A_0} \tag{3.3}$$

where, $A_0 = \omega_n{}^2 = k/m$, $A_1 = \omega_n / Q = 2\zeta\omega_n = b/m$, and $B_1 = B_0 / m$.

This transfer function can be represented by a state space equation as:

$$\begin{aligned} \dot{x} &= Ax + BV \\ y &= Cx \end{aligned} \tag{3.4}$$

where, $x = [z \quad \dot{z}]^T$ is the state vector representing the position and velocity of the vibrating probe tip, V is the control input (i.e. applied voltage), y is the output vector, and the matrices A, B, and C are defined as

$$A = \begin{bmatrix} 0 & 1 \\ -A_0 & -A_1 \end{bmatrix},\ B = \begin{bmatrix} 0 \\ B_1 \end{bmatrix},\ C = [0 \quad 1] \tag{3.5}$$

3.2 State Feedback

Full state feedback, also known as pole placement, is a method employed in feedback control system theory to place the closed loop poles of a plant in predetermined locations in the complex plane. The location of the poles is related to the selection of the eigenvalues of the system, which control the characteristics of the dynamical response of the system. The poles of the system are the roots of the characteristic equation given by $|sI - A| = 0$. Full state feedback is achieved by defining an input vector proportional to the state vector as $V = -Kx$, where $K = [H \quad G]$ is the gain vector. Now, the roots of the full state feedback system are given by the characteristic equation $|sI - (A - BK)| = 0$. By selecting proper gains for the vector *K*, we can place the poles of the closed loop system to the desired locations. If Ackermann's approach is utilized for the pole placement, the gain vector *K* is calculated as

$$K = [0 \quad 1] P_C^{-1} \, q(A) \tag{3.6}$$

where, $P_c = [B \quad AB]$ is the controllability matrix and $q(A) = A^2 + A_1^{des} A + A_0^{des} I$ is the desired characteristic equation. The rank of the matrix P_c is 2 in our case, indicating a fully controllable system. Hence, the vector *K* for our system can be calculated as

$$K = \begin{bmatrix} H & G \end{bmatrix} = \frac{1}{B_1}\begin{bmatrix} A_0^{des} - A_0 & A_1^{des} - A_1 \end{bmatrix} = \frac{m}{B_0}\left[(\omega_n^{des\,2} - \omega_n^2) \quad (\frac{\omega_n^{des}}{Q^{des}} - \frac{\omega_n}{Q}) \right]$$
$$= \frac{1}{B_0}\begin{bmatrix} (k^{des} - k) & (b^{des} - b) \end{bmatrix} \tag{3.7}$$

This result is not unexpected if the equation of motion of the probe, equation 3.1, is inspected carefully (note that $k^{des} = k \pm H$ and $b^{des} = b \pm G$ for position and velocity feedback).

3.3 Estimating the Transfer Function of the Cantilever Probe

In order to estimate the feedback gains *H* and *G*, which can be used in the electronic circuit shown in figure 2.7 to alter the resonance frequency and the *Q* factor of the probe, first, a transfer function of the probe is developed based on the frequency sweep data and then the gains are calculated using the pole placement approach implemented in MATLAB. For this purpose, the probe is driven by a sinusoidal input voltage at different frequencies around the resonance frequency of 224 kHz (note that the first three resonance frequencies of the probe are far away from each other and there is no coupling between them [12]) and the amplitude of the probe velocity is measured experimentally using the LDV. We then developed an iterative curve fitting algorithm to identify the parameters of the transfer function given in Eq. (3.3). The parameters of interest in the transfer function are A_0, A_1,

and B_1. Since the resonant frequency of the probe, ω_n, can be determined directly via frequency sweep, A_0 is known in advance, and we only need to determine the parameters A_1 and B_1. The parameter B_1 affects the system gain only while A_1 affects both the gain and the damping ratio. We calculate B_1 and A_1 by curve fitting to the experimental amplitude curve. For this purpose, we iterate A_1 and B_1 until the estimated curve matches the experimental one with a small acceptable error (see Figure 3.1). The error is defined as the difference between the areas under the estimated and experimental curves and the aim of the curve fit algorithm is to minimize this error down to an acceptable value through the iterations. Once the parameters of the transfer function is estimated, the gain vector $K = [H \quad G]$ for the desired resonance frequency and the desired quality factor can be calculated in MATLAB using the pole placement approach discussed in chapter 3.2.

The pseudo code of the iterative curve fitting algorithm to identify the parameters of the transfer is as follows:

Determine $A_0 = \omega_n^2$ *from the experimental amplitude curve*

Assign initial values for

Constants:

$\Delta\zeta = 0.1$ *(choose a small number)* // *decrement in damping ratio*

$e_{ths} = 1$ *(choose a small number)* // *threshold in percent relative error*

Variables:

$\zeta = 0.01$ *(choose a small number initially)* // *damping ratio*

e = 999999.9 (choose a large number initially) // percent relative error

B_1 = 0.01 (choose a small number initially)

$A_1 = 2\zeta\omega_n$

Generate the estimated amplitude curve using the transfer function

while abs(e) > e_{ths}

Calculate

e =100 (area under the estimated amplitude curve – area under the experimental amplitude curve)/ area under the experimental amplitude curve;*

B_1 = peak value of the experimental amplitude curve / peak value of the estimated amplitude curve;

$\zeta = \zeta - (\Delta\zeta * e)$;

$A_1 = 2\zeta\omega_n$;

Generate the estimated amplitude curve using the transfer function

end

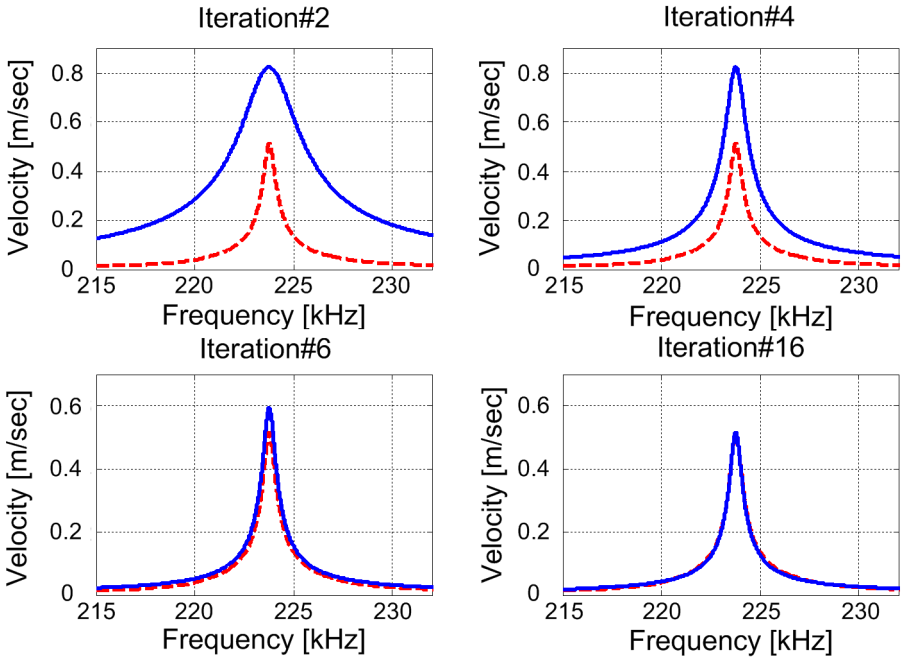

Figure 3.1: Snapshots showing the curve fitting approach used to estimate the parameters of the transfer function of the probe. The red dashed curve represents the experimental data, whereas the blue solid one is the estimated curve.

Chapter 4

SIMULATION MODEL

Simulating the dynamical behavior of the cantilever alone does not help us to investigate the scan performance under state feedback control for different scan settings. We also developed the models of the individual scan components and then integrated them with the model of the cantilever using SIMULINK to perform end to end scanning simulations. [19]

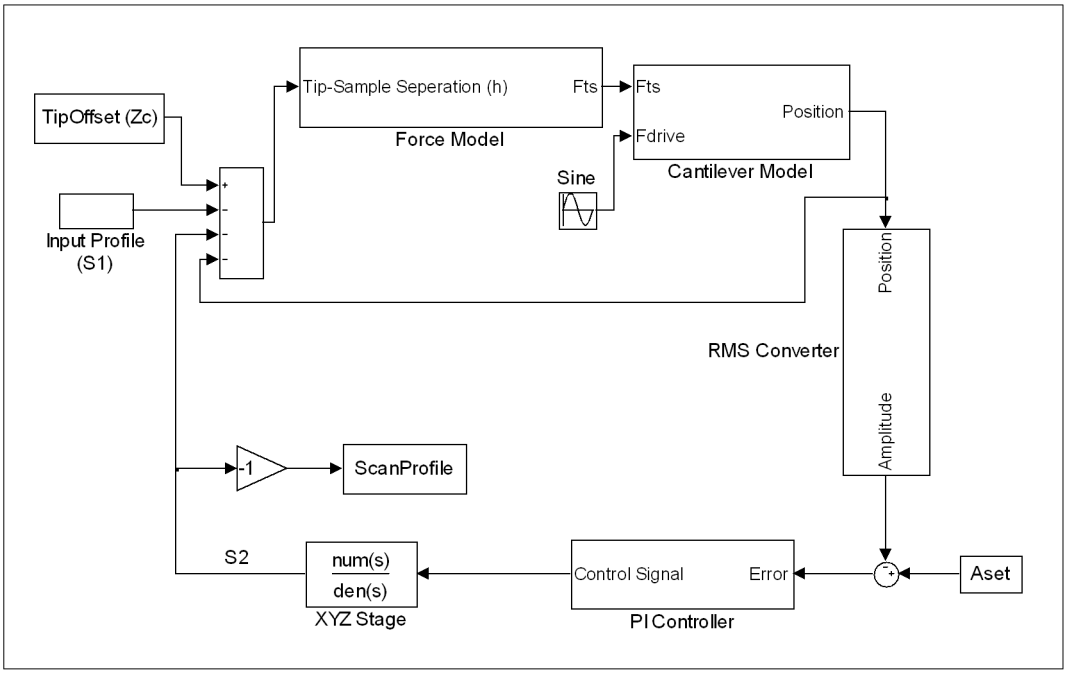

Figure 4.1: SIMULINK model of the scanning system.

4.1. Models of the Physical Components in the Setup

4.1.1 Force Model

The force interactions between the probe tip and sample geometry is modeled as a spherical object interacting with a flat surface [20-22]. In the tapping mode AFM, the cantilever is oscillated over the sample surface and contacts the surface for a brief period of time at each oscillation cycle. As a result, the distance h between the cantilever tip and sample surface changes continuously. Depending on the separation distance, two different interaction models are typically utilized to calculate the tip-sample forces.

Non-contact Forces: For the separation distances larger than the inter-atomic distance, a_0, the long range attractive force is dominant (note that electrostatic interactions are ignored). The attraction results from the integration of van der Waals energy between two atoms over the atoms of interacting surfaces. The van der Waals attraction force between a sphere and a flat surface is the negative gradient of this energy and can be written as a function of tip-sample separation distance h, the tip radius R, and the Hamaker constant H as follows [23]

$$F_{vdw}(h) = \frac{HR}{h^2} \qquad \text{if } h > a_0 \tag{4.1}$$

Contact Forces: It is assumed that a mechanical contact between the cantilever tip and the sample surface occurs when the separation distance h is smaller than the inter-atomic distance, a_0, (negative values of h indicate indentation into the sample surface). During the contact, both adhesive and repulsive forces are effective. According to the DMT theory [24], the adhesion force is equal to the van der Waals attraction force when $h = a_0$. The repulsive force arising from the mechanical contact of the tip with the sample surface is modeled using contact mechanics. Hence, the total force acting on the cantilever tip due the adhesive and repulsive components is given by

$$F_{contact}(h) = -\frac{HR}{6{a_0}^2} + \frac{4}{3}E^*\sqrt{R}(a_0 - h)^{3/2} \qquad \text{if } h < a_0 \tag{4.2}$$

$$\frac{1}{E^*} = \frac{(1-\nu_t)^2}{E_t} + \frac{(1-\nu_s)^2}{E_s} \tag{4.3}$$

where E^* is the effective young's modulus of the tip-sample pair, E_t and E_s are the elastic moduli of the tip and surface material, ν_t and ν_s are the Poisson's ratio of the tip and the surface material, respectively.

Combining the contact and non-contact forces, the interaction force F_{ts} between the tip and the surface can be expressed as:

$$F_{ts}(h) = \begin{cases} -\dfrac{HR}{h^2} & \text{if } h > a_0 \\ -\dfrac{HR}{6a_0^{\,2}} + \dfrac{4}{3}E^*\sqrt{R}(a_0 - h)^{3/2} & \text{if } h < a_0 \end{cases} \qquad (4.4)$$

Force model is established using equation 4.4. Switch enables the use of either non-contact forces or contact forces depending on *h*.

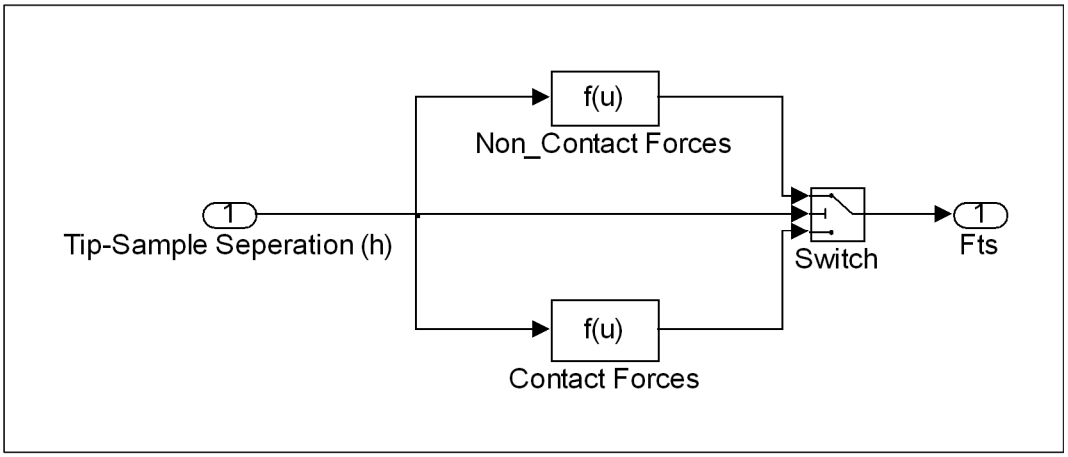

Figure 4.2: Force model built in SIMULINK.

4.1.2 Cantilever Model

Cantilever model block is constructed in SIMULINK as a mass spring damper model as was told in chapter 3.1. We have to construct the block as the transfer function between the force applied to the probe tip, *F(s)*, and the position of the probe tip, *z(s)* in order to add the tapping forces to the excitation signal. Since we know $A_0 = \omega_n^{\,2} = k/m$, $A_1 = \omega_n / Q = 2\zeta\omega_n = b/m$, and $B_1 = B_0/m$, in order to construct model in equation 3.2 we have to know at least one of the parameters (i.e. effective mass, damping, and stiffness) to find others. We use nominal value for the stiffness of the probe, $k = 3\,N/m$, as it is told by the manufacturer to find effective mass and damping using A_0 and A_1. State feedback control is applied by modifying the effective damping (b_{new} in figure 4.3) and effective stiffness (k_{new} in figure 4.3) according to the state feedback gain vector, i.e. $bnew = b - G$ and $k_{new} = k - H$

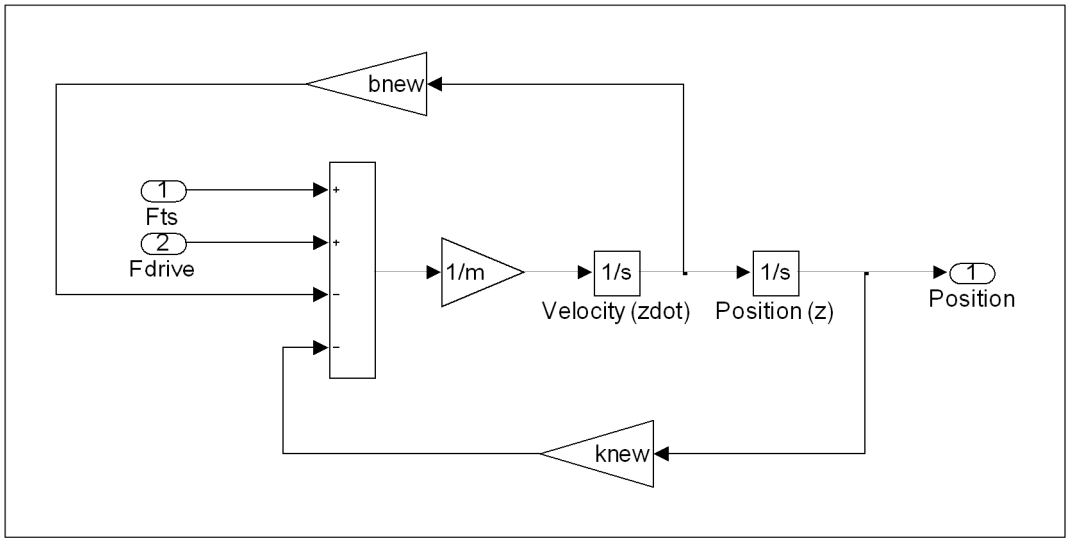

Figure 4.3: Cantilever model built in SIMULINK.

4.1.3 RMS Converter

This block is used to compute the rms of the vibration position. A built-in SIMULINK block (RMS in SimPowerMechanics Library) is used for this operation and the RMS value of the input signal is calculated over a running window. In order to calculate the oscillation amplitude of the cantilever, the RMS of the position signal is multiplied by a proper gain K that is $\sqrt{2}$ as shown in figure 4.4.

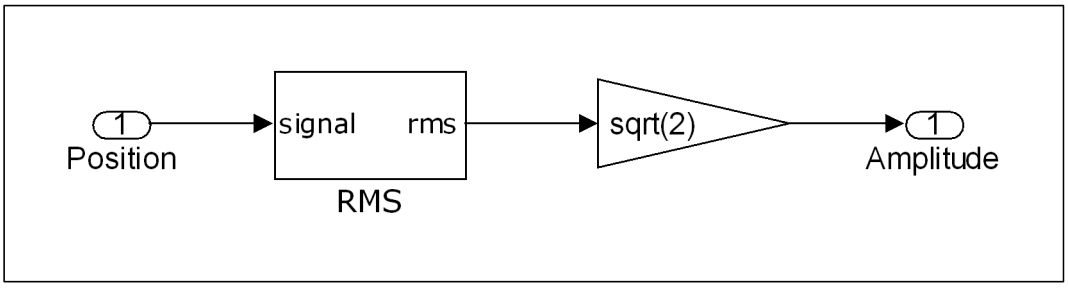

Figure 4.4: RMS model built in SIMULINK.

4.1.4 PI Scan Controller

This block is used to control the vertical movements of the computer controlled XYZ stage. Well known PI control utilized to actuate the XYZ stage based on the error in the peak to peak amplitude of the cantilever oscillations ($A_{set} - A_p$).

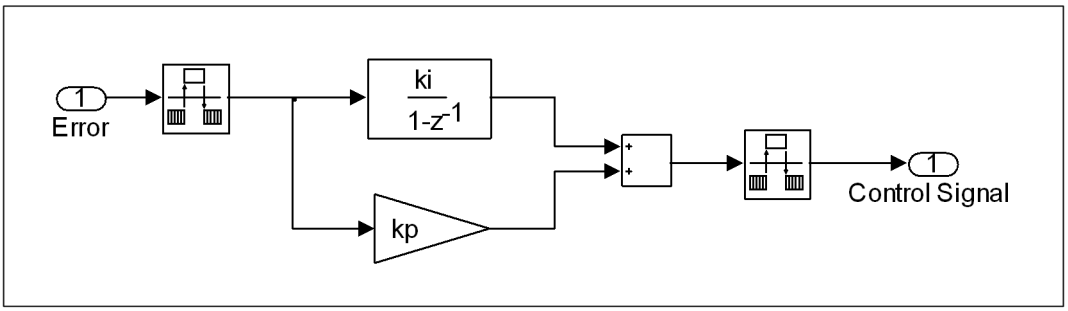

Figure 4.5: PI scan controller built in SIMULINK

4.1.5 XYZ Stage

In order to model the dynamics of the computer controlled XYZ nano stage used in the physical setup, we have used a first order transfer function with a time constant smaller than the sampling time of the PI controller. The vertical movements of the XYZ stage are represented as S_2 in figure 4.1.

4.2. Models for Input/Output Operations

In addition to the models of above components, the following blocks are used for regulating input output operations

4.2.1 Input Profile

This block generates the input surface profile as a function of time. In the case of scanning calibration steps with a constant height of h_s (in our case $h_s = 100nm$) and width of w_s, the input profile is periodic with a period of $t_s = w_s / v_s$, where v_s is the scan speed. For the time interval $0 < t < t_s$ input profile (S_1) is given by 0 for $0 < t < t_s/2$ and h_s for $t_s/2 < t < t_s$

4.2.2 Output Profile

This is the block where the inverse of the movements of the XYZ stage are recorded. Hence, this is the output of the scanning system. The output scan profile should exactly match the desired input profile under ideal conditions.

Chapter 5

EXPERIMENTS

5.1 Effect of State Gains on the Probe Response

We investigated the effect of position and velocity gains on the response of the probe. The resonance frequency and the damping characteristics of the system can be set by adjusting the position and velocity gains.

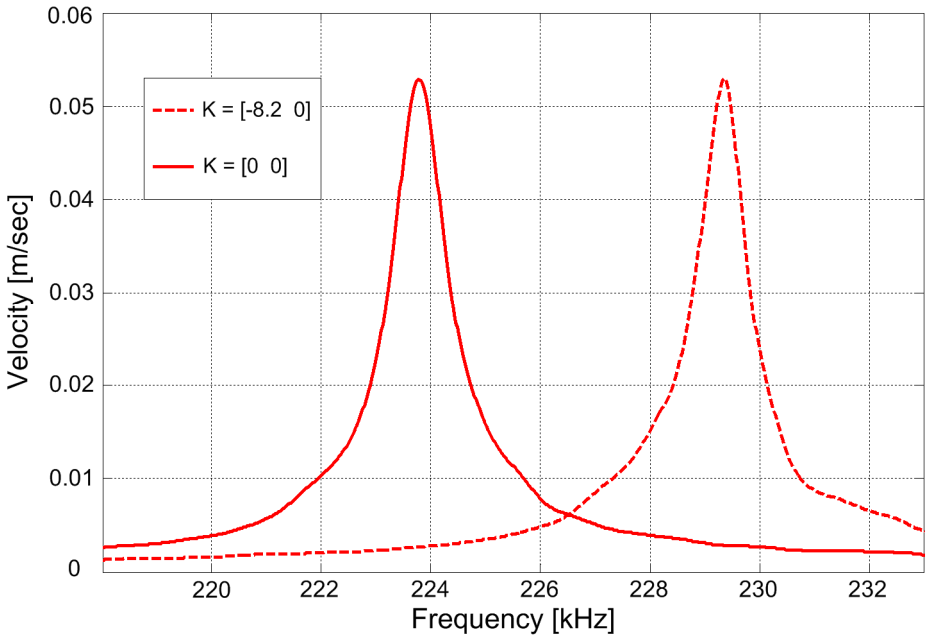

Figure 5.1: Effect of position feedback on resonance frequency.

The effect of position feedback on the probe dynamics can be seen in figure 5.1. It causes a shift in resonance frequency as expected.

Velocity is the other state that is fed back to the system to change the effective damping of the probe and also Q factor of the probe. (see figure 5.2)

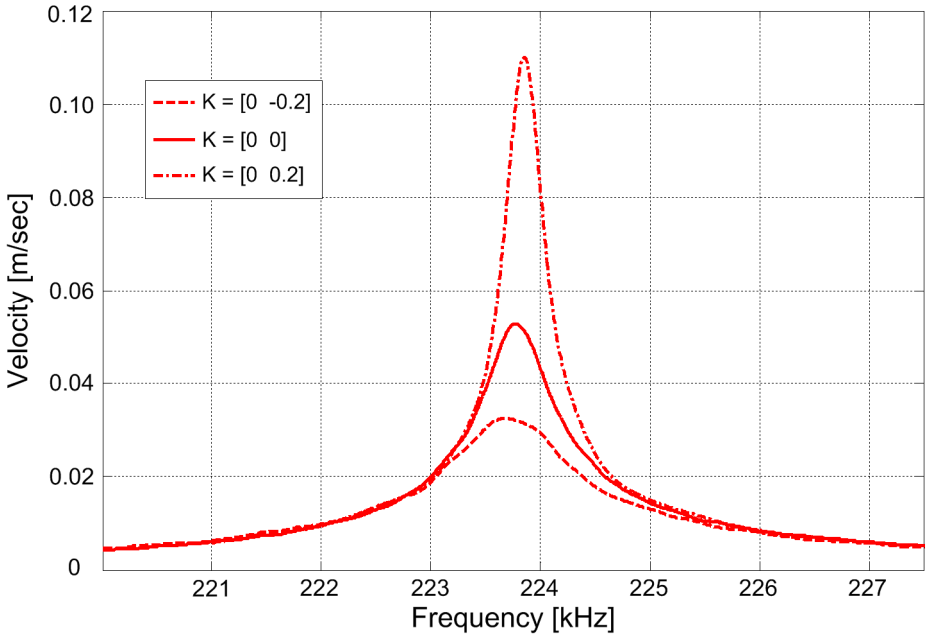

Figure 5.2: Effect of velocity feedback on *Q* factor.

In figure 5.3, we show the combined effect of changing velocity and position gains for adjusting the effective *Q* factor and resonance frequency of the probe simultaneously. Note that the numerical model (blue solid line) shows excellent agreement with the experimental

data (red dashed line). As shown in the figure 5.3, the resonance frequency of the probe is shifted to the right and its effective Q factor is reduced at the same time to decrease the time constant and hence improve its response time.

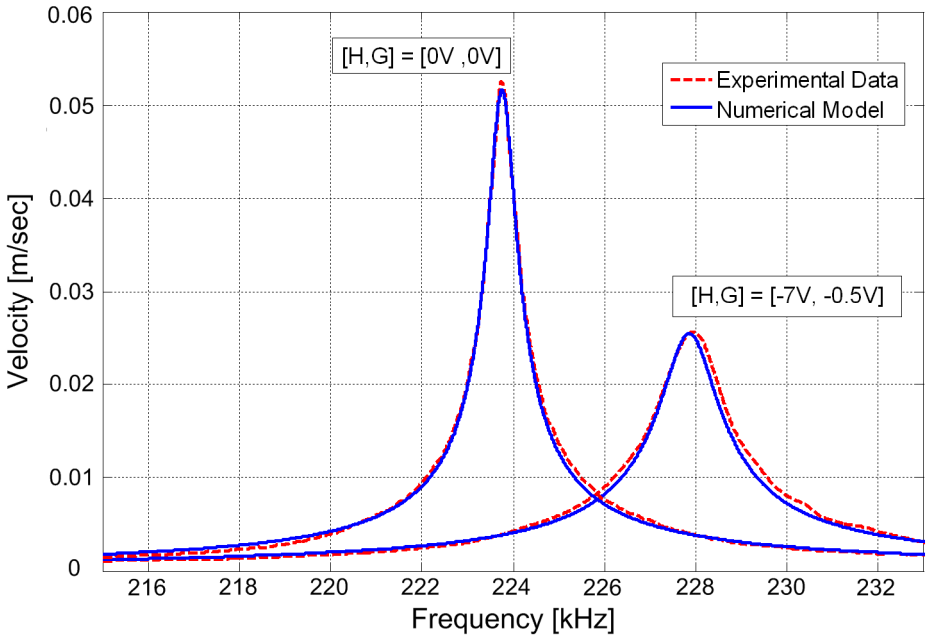

Figure 5.3: The resonance frequency and the Q factor of the probe are set to the desired values by altering the position and velocity gains simultaneously.

In figure 5.4, the effect of position gain H on the resonance frequency and the Q factor of the probe and also the effect of velocity gain G on the Q factor of the probe are plotted.

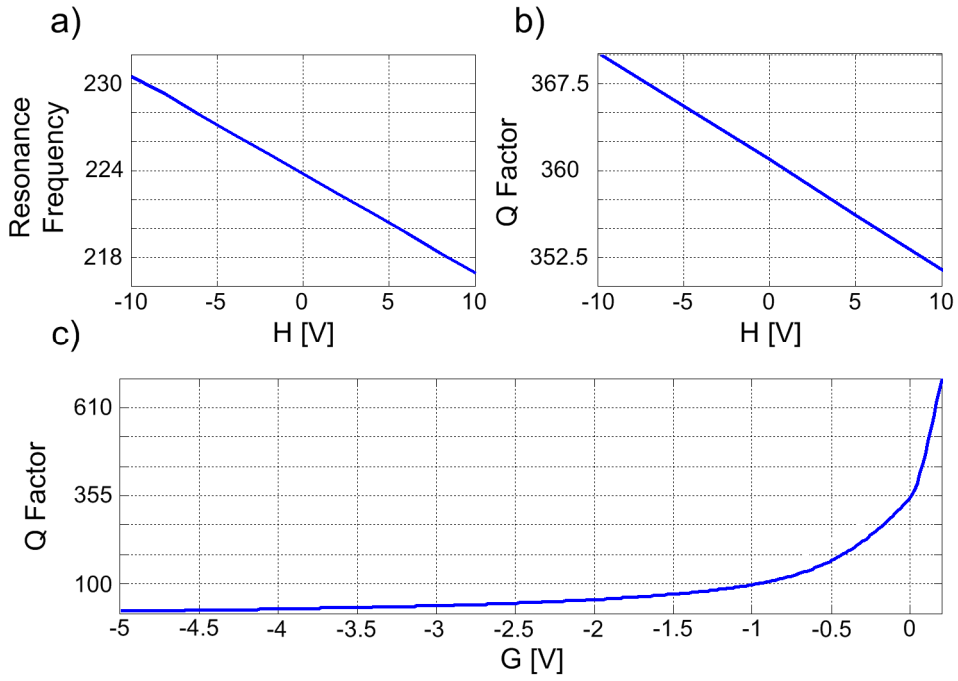

Figure 5.4: The relation (a) between the position gain H and the resonance frequency, (b) between the position gain H and the Q factor, and (c) between the velocity gain G and the Q factor of the probe.

To further analyze the transient response of the probe, the effect of altering G and H gains on the time constant of the probe, τ, is also investigated using the numerical model. Figure 5.5 shows the percent change in time constant of the probe as the gains G and H are altered. In general, decreasing the position gain H (i.e. increasing the resonance frequency) and/or decreasing the velocity gain G (i.e. decreasing the Q factor) has a positive effect of

reducing the time constant, but the influence of resonance frequency on the time constant is less significant at negative values of gain *G*.

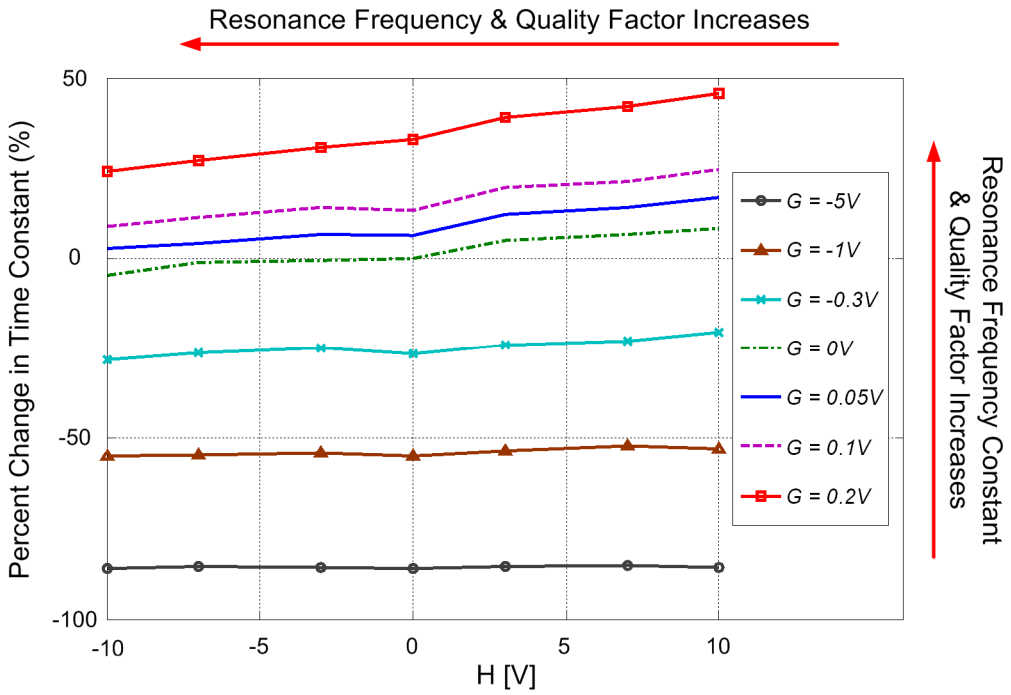

Figure 5.5: The effect of state gains on the time constant of the probe.

5.2. Effect of State Gains on the Scan Profile

The effect of gain settings on the scan results is investigated using a SIMULINK model and the numerical simulations are verified via real experiments. For this purpose, the transfer function of the probe developed in chapter 3 is inserted into our SIMULINK model (see the

details of this model in Varol et al. [13]) and then the feedback loops for position and velocity are added. Using this model, we simulate the process of scanning 100nm steps (width = 1.5µm) in tapping mode AFM and investigate the effect of state gains on the scan error (see figure 5.6). The scan error is calculated by first integrating the positional error between the profile obtained from the SIMULINK model and the desired profile over a step width and then normalizing the sum by the area under the step [13].

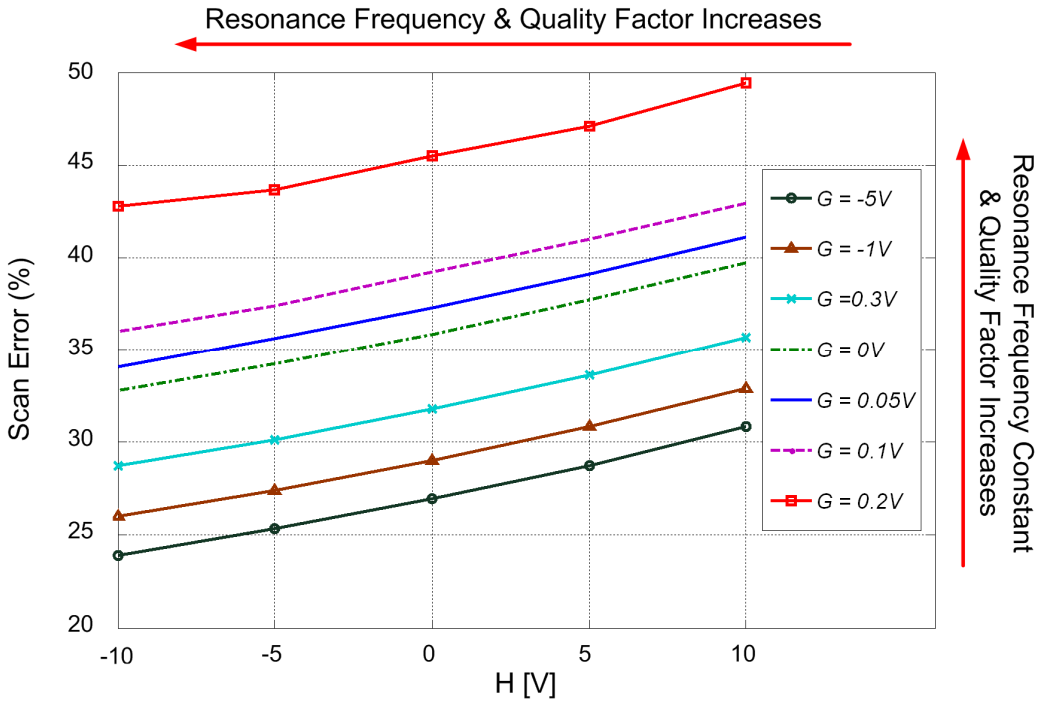

Figure 5.6: The effect of state gains on the scan error is investigated using the SIMULINK model.

As shown in figure 5.6, the scan error is reduced as the resonance frequency is increased and/or the Q factor is decreased (note that both alterations reduce the time constant of the probe and improves its response time).

To verify the numerical simulations, we performed scan experiments in tapping mode using our AFM setup. A calibration grating having periodic steps of 100nm (TGZ02, range: 94nm-106nm, Mikromash, USA) is scanned at two different scan speeds (v_1 = 4μm/s and v_2 = 20μm/s) using the experimental setup. In figure 5.7, we compare the scans obtained by the probe having a high Q factor ($K = [0 \quad 0.3]$) versus the probe having a low Q factor and higher resonance frequency ($K = [-6.5 \quad -1.5]$). As shown in figure 5.7.a, the response of the probe having low time constant (red dashed line) is better than the one having higher time constant (blue dashed line). The probe responds faster to the same step when its time constant is reduced using the state feedback control. The response of the probe at high scan speeds is slow and causes an inclined profile for the upward and downward steps (see figure 5.7.b). As the scanning speed increases the positive effect of the state feedback control decreases, but still exists.

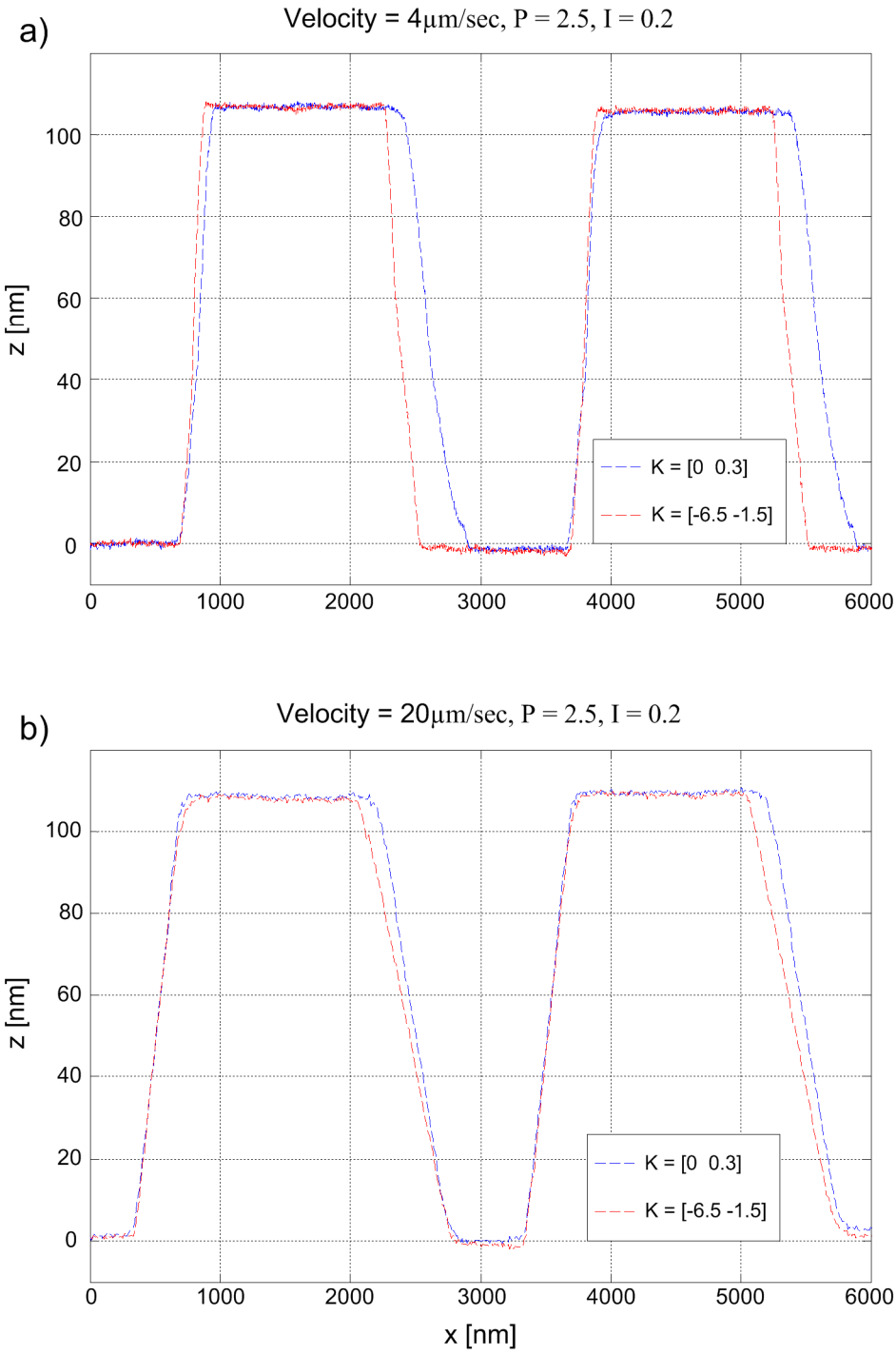
a)
Velocity = 4μm/sec, P = 2.5, I = 0.2
z [nm]
0
20
40
60
80
100
0
1000
2000
3000
4000
5000
6000
K = [0 0.3]
K = [-6.5 -1.5]
b)
Velocity = 20μm/sec, P = 2.5, I = 0.2
z [nm]
x [nm]
K = [0 0.3]
K = [-6.5 -1.5]

Figure 5.7: The effect of state gains on the scan error is investigated experimentally using a calibration grating having periodic steps. The dashed blue and red lines represent the response of the probe having high and low time constants, respectively. Note that the control parameters for the XYZ scanner are the same in both cases (P = 2.5, I = 0.2).

Instead of applying state feedback control to the cantilever probe, one can also increase the proportional gain P of the XYZ scanner to make the upward and downward steps sharper during a scan, but this also results in more oscillations and overshoots in the scanner response and frequent sticking of the probe to the surface (see figure 5.8.a). In figure 5.8.b, we compare the scan results obtained at high proportional gain P for the probe having high (blue solid line) and low (red solid line) time constants. As it can be seen, the state feedback control of the probe decreases the overshoots, prevents the probe from sticking to the surface, and hence results in better scan profile.

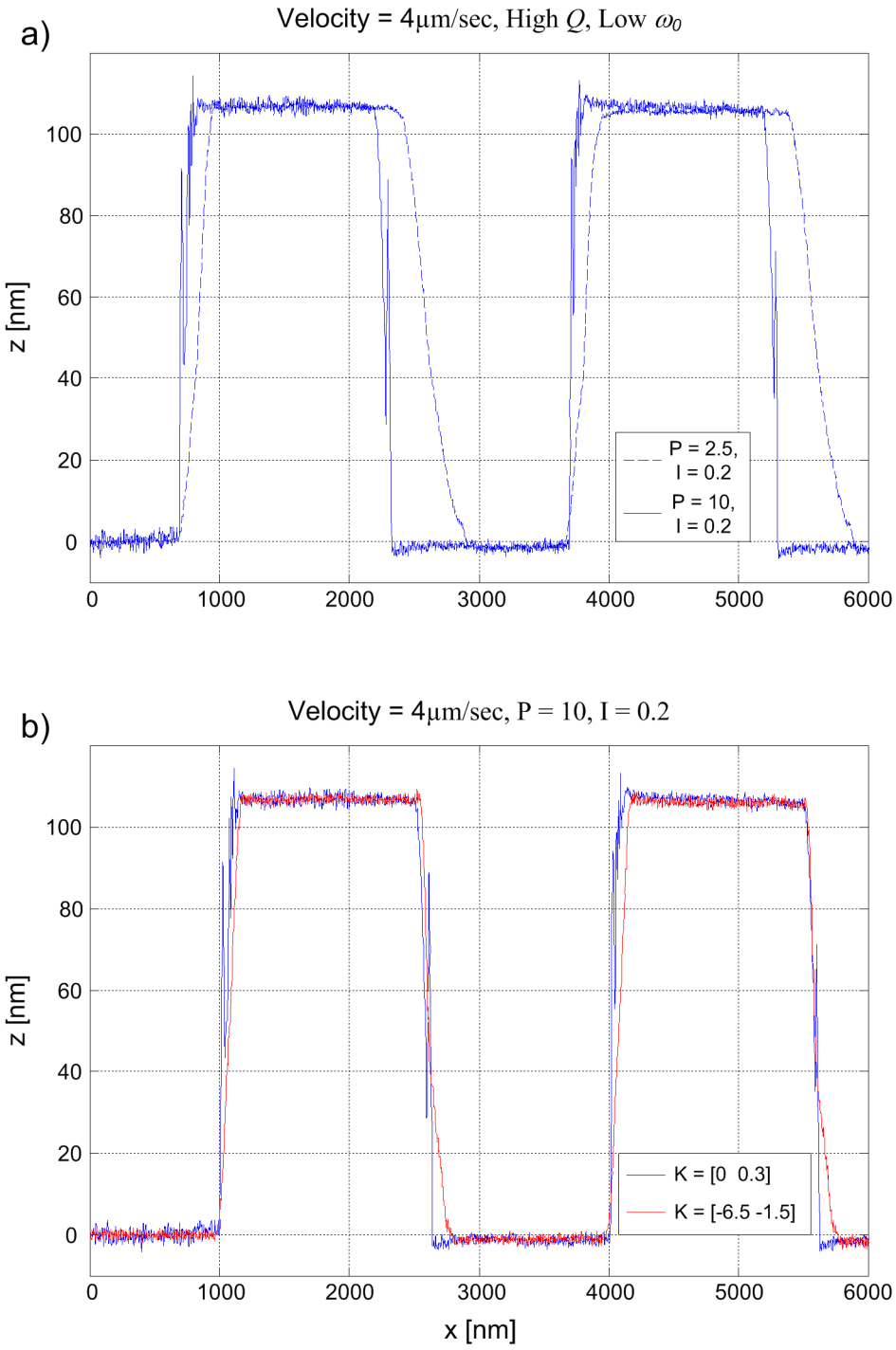
a)
Velocity = 4μm/sec, High Q, Low ω_0
z [nm]
0
20
40
60
80
100
0
1000
2000
3000
4000
5000
6000
P = 2.5,
I = 0.2
P = 10,
I = 0.2
b)
Velocity = 4μm/sec, P = 10, I = 0.2
z [nm]
x [nm]
K = [0 0.3]
K = [-6.5 -1.5]

Figure 5.8: (a) The effect of increasing the proportional gain P of the XYZ scanner on the scan results (b) The effect of state feedback control of probe on the scan results at high proportional gain P = 10.0.

While reducing the time constant of the probe (by increasing its resonance frequency and/or reducing the Q factor), decreases the scan error, it also increases the tapping forces applied by the probe on the sample. Since measuring these forces experimentally is highly difficult, we investigate the effect of state gains on the tapping forces through numerical simulations. As shown in figure 5.9, the tapping forces increase as the resonance frequency is increased and/or the Q factor is decreased. The tapping force is calculated using the average of maximum indentations of the probe tip into the sample surface after the tapping amplitude reaches steady state.

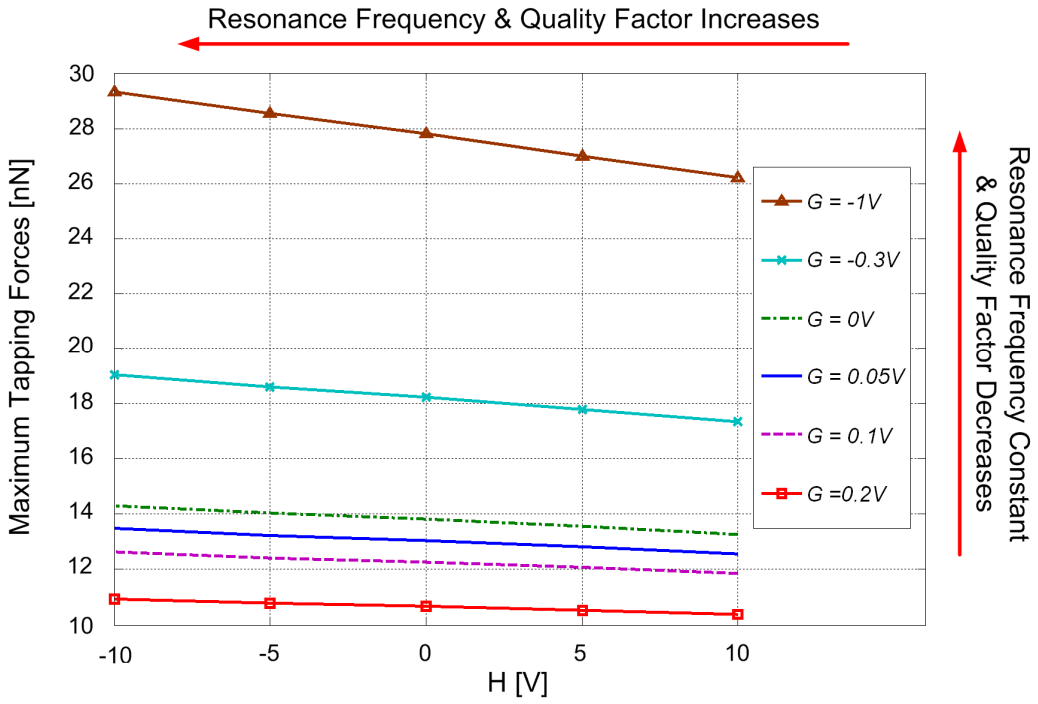

Figure 5.9: The effect of state gains on the tapping forces is investigated using the numerical model.

Chapter 6

DISCUSSION and CONLUSION

We presented an approach for adjusting the resonance frequency and the Q factor of an AFM probe using state feedback control. For this purpose, an analog circuit was built to change the effective stiffness and damping of the probe. While changing the damping affects the Q factor of the probe only, a change in the stiffness modifies both the resonance frequency and the Q factor. For this reason, it is important to change the effective stiffness and the damping of the probe simultaneously using a state feedback controller, which enables us to select the poles of the transfer function representing the probe based on the desired values of the Q factor and ω_n. To implement the state feedback control in dynamic AFM, it was necessary to obtain the full state (position and velocity) of the probe as a function of time. Since the LDV can only measure the velocity of the oscillating probe, we built an analog integrator circuit to obtain the position signal from the measured velocity signal through integration. We then calculated the position and velocity gains (H and G) that must be used in the feedback loop to achieve the desired values of ω_n *and* Q factor, respectively. For this purpose, we first estimated the transfer function of the probe using the frequency sweep data and then applied the pole placement technique as discussed in

chapter 3. Through this analysis, we observed that the magnitude of the positional gain H in our system is significantly higher than that of the velocity gain G. It was obvious that this high gain H could not be provided by the voltage supply directly. We provided the major part of this gain through the integrator circuit and the rest is delivered by the voltage supply.

We performed scan experiments with probes having high and low time constants by adjusting the feedback gains. The results of these experiments showed that as the time constant of the probe is reduced (and hence the response of the probe is faster), the scan error is reduced and image quality is improved. While the same effect can be achieved by increasing the proportional gain of the XYZ scanner, this also results in more oscillations and overshoots in scanner response and frequent sticking of the probe to the surface. In order to reduce the time constant of the probe, we simultaneously reduced its Q factor and increased its resonance frequency. However, the results of our numerical simulations showed that this also increases the magnitude of the tapping forces, which is not desirable.

Instead of using the pole placement approach to set the feedback gains, an optimum controller can also be designed such that the scan error and/or the tapping forces are minimized. Our study shows that there is a tradeoff between the scan error and the tapping forces. Attempting to reduce the scan error by reducing the Q factor and increasing ω_n

causes the tapping forces to increase. Hence, an optimum controller can be a remedy to this problem. Moreover, as an alternative to building an analog integrator circuit, a state observer could be used to estimate the position signal from the measured velocity signal. For example, Sebastian et al. [16] estimate the velocity from the measured position signal using a state observer. In our setup, a DAQ card with a high sampling rate is required for the realization of a state observer since the operating frequency of our probe is quite high (around 224kHz). Implementation of a state observer will be the subject of our future research.

BIBLIOGRAPHY

[1] Fantner G. E. , Schitter G., Kindt J. H., Ivanov T., Ivanova K., Patel R., Holten-Andersen N., Adams J., Thurner P. J., Rangelow I. W., and Hansma P. K., "Components for high speed atomic force microscopy", vol. 106, pp. 881, *Ultramicroscopy*, **2006**.

[2] Albrecht T. R., Grtitter P., Horne D., and Rugar D., "Frequency modulation detection using high-Q cantilevers for enhanced force microscope sensitivity", vol. 69, pp. 668, *Journal of Applied Physics*, **1991**.

[3] Mertz J., Marti 0., and Mlynek J., "Regulation of a microcantilever response by force feedback", vol. 62, pp. 2344, *Applied Physics Letters*, **1993**.

[4] Sulchek T., Hsieh R., Adams J. D., Yaralioglu G. G., Minne S. C., Quate C. F., Cleveland J. P., Atalar A., and Adderton D. M., "High-speed tapping mode imaging with active Q control for atomic force microscopy", vol. 76, pp. 1473, *Applied Physics Letters*, **2000**.

[5] Rodriguez T. R., and Garcia R., "Theory of Q control in atomic force microscopy", vol. 82, pp. 4821, *Applied Physics Letters*, **2003**.

[6] Chen L., Yu X., and Wang D., "Cantilever dynamics and quality factor control in AC mode AFM height measurements", vol. 107, pp. 275, *Ultramicroscopy*, **2007**.

[7] Kokavecz A. J., and Horvath Z. L., "Dynamical properties of the Q-controlled atomic force microscope", vol. 85, pp. 3232, *Applied Physics Letters*, **2004.**

[8] Ebeling D., Hölscher H., Fuchs H., Anczykowski B., and Schwarz U. D., "Imaging of biomaterials in liquids: a comparison between conventional and Q-controlled amplitude modulation ('tapping mode') atomic force microscopy", vol. 17, pp. 221, *Nanotechnology*, **2006**.

[9] Jaggi R. D., Obregon A. F., Studerus P., and Ensslin K., "Detailed analysis of forces influencing lateral resolution for Q-control and tapping mode", vol. 79, pp. 135, *Applied Physics Letters*, **2001**.

[10] Hölscher H., Ebeling D., and Schwarz U. D., "Theory of Q-Controlled dynamic force microscopy in air", vol. 99, pp. 084311, *Journal of Applied Physics*, **2006**.

[11] Hölscher H., and Schwarz U. D., "Theory of amplitude modulation atomic force microscopy with and without Q-Control", vol. 42, pp. 608, *International Journal of Non-Linear Mechanics*, **2007**.

[12] Gunev I., Varol A., Karaman S., and Basdogan C., "Adaptive Q control for tapping-mode nanoscanning using a piezoactuated bimorph probe" vol. 78, pp. 043707, *Review of Scientific Instruments*, **2007**.

[13] Varol A., Gunev I., Orun B., and Basdogan C., "Numerical simulation of nano scanning in intermittent-contact mode AFM under Q control", vol. 19, pp. 075503, *Nanotechnology*, **2008**.

[14] Viani M. B., Schaffer T. E., Chand A., Rief M., Gaub H. E., and Hansma P. K., "Small cantilevers for force spectroscopy of single molecules", vol. 86, pp. 2258, *Journal of Applied Physics*, **1999**.

[15] Stark R. W., Schitter G., Stark M., Guckenberger R., and Stemmer A., "State-space model of freely vibrating and surface-coupled cantilever dynamics in atomic force microscopy", vol. 69, pp. 085412, *Physical Review B*, **2004**.

[16] Sebastian A., Sahoo D. R., and Salapaka M. V., "An Observer Based Sample Detection Scheme for Atomic Force Microscopy", pp. 2132, *Proceedings of the 42nd IEEE Conference on Decision and Control*, **2003**.

[17] Sahoo D. R., De T., and Salapaka M. V., "Observer based imaging methods for Atomic Force Microscopy", pp. 1185, *Proceedings of the 44th IEEE Conference on Decision and Control, and the European Control Conference*, **2005**.

[18] Gunev I., "Adaptive Q-control for Tapping-mode Nano Scanning Using a Piezo-actuated Bimorph Probe", *MSc. Thesis, Koc University*, 2006.

[19] Varol A., "Numerical Simulation of Nano Scanning in Tapping Mode AFM under Q control", *MSc. Thesis, Koc University*, 2007.

[20] Perez R., Stich I., Payne M. C. and Terakura K., "Surface-tip interactions in noncontact atomic-force microscopy on reactive surfaces: Si(111)", vol. 58, pp. 10835, *Physical Review B*, **1998**

[21] García R. and San Paulo A., “Attractive and repulsive tip-sample interaction regimes in tapping-mode atomic force microscopy”, vol. 60, pp. 4961, *Physical Review B*, **1999**.

[22] Aimé J. P., Boisgard R., Nony L., and Couturier G., “Nonlinear Dynamic Behavior of an Oscillating Tip-Microlever System and Contrast at the Atomic Scale”, vol. 82, pp. 3388, *Physical Review Letters*, **1999**.

[23] Israelachvili J., “Intermolecular and Surface Forces”, *Academic, London*, **1995**.

[24] Derjagurin B.V., Muller V.M., Toporov Y.P., “Effects of contact deformations on the adhesion of particles”, vol. 53, pp.314, *Journal of Colloid Science*, **1975**.